Heliyon 10 (2024) e25716

Contents lists available at ScienceDirect

Heliyon

journal homepage: www.cell.com/heliyon

Research article

SMG9 is a novel prognostic-related biomarker in glioma correlating with ferroptosis and immune infiltrates

Yong Dai [a,b,1], Huan Zhang [a,b,1], Sujuan Feng [a,b,1], Chao Guo [a,b], Wenjie Tian [a,b], Yimei Sun [a,**], Yi Zhang [a,*]

[a] *Department of Neurosurgery, Affiliated Hospital 2 of Nantong University and First People's Hospital of Nantong City, No. 666 Shengli Road, Nantong 226001, China*

[b] *State Key Laboratory of Systems Medicine for Cancer, Shanghai Cancer Institute & Renji Hospital Affiliated to Shanghai Jiao Tong University School of Medicine, Shanghai 200025, China*

ARTICLE INFO

Keywords:
CGGA
TCGA
SMG9
Glioma
Ferroptosis

ABSTRACT

Background: Glioma is the most frequent type of malignancy that may damage the brain with high morbidity and mortality rates and patients' prognoses are still dismal. Ferroptosis, a newly uncovered mode of programmed cell death, may be triggered to destroy glioma cells. Nevertheless, the significance of ferroptosis-related genes (FRGs) in predicting prognosis in glioma individuals is still a mystery.

Methods: The CGGA (The Chinese Glioma Atlas), GEO (Gene Expression Omnibus), and TCGA (The Cancer Genome Atlas) databases were all searched to obtain the glioma expression dataset. First, TCGA was searched to identify differentially expressed genes (DEGs). This was followed by a machine learning algorithm-based screening of the glioma's most relevant genes. Additionally, these genes were subjected to Gene Ontology (GO) and KEGG (Kyoto Encyclopedia of Genes and Genomes) functional enrichment analyses. The chosen biological markers were then submitted to single-cell, immune function, and gene set enrichment analysis (GSEA). In addition, we performed functional enrichment and Mfuzz expression profile clustering on the most promising biological markers to delve deeper into their regulatory mechanisms and assess their clinical diagnostic capacities.

Results: We identified 4444 DEGs via differential analysis and 564 FRGs from the FerrDb database. The two were subjected to intersection analysis, which led to the discovery of 143 overlapping genes. After that, glioma biological markers were identified in fourteen genes by the use of machine learning methods. In terms of its use for clinical diagnosis, SMG9 stands out as the most significant among these biomarkers.

Conclusion: In light of these findings, the identification of SMG9 as a new biological marker has the potential to provide information on the mechanism of action and the effect of the immune milieu in glioma. The promise of SMG9 in glioma prognosis prediction warrants more study.

* Corresponding author. Department of Neurosurgery, Affiliated Hospital 2 of Nantong University and First People's Hospital of Nantong City, No. 666 Shengli Road, Nantong 226001, China.

** Corresponding author. Department of Neurosurgery, Affiliated Hospital 2 of Nantong University and First People's Hospital of Nantong City, No. 666 Shengli Road, Nantong 226001, China.

E-mail addresses: 502730687@qq.com (Y. Sun), zhangyi9285@sina.com (Y. Zhang).

[1] These authors contribute equally.

https://doi.org/10.1016/j.heliyon.2024.e25716

Received 19 August 2023; Received in revised form 19 January 2024; Accepted 1 February 2024

Available online 8 February 2024

1. Introduction

Glioma is the most prevailing type of cancer that affects the central nervous system (CNS) [1,2]. Recently, there have been many advances in the treatment of glioma, including surgical resections, chemoradiotherapy, gene therapy, and immunotherapy [3–6]. However, it is unfortunate that the prognosis for those who have been diagnosed with glioma is still not promising, with a median survival duration of only 9–15 months [7–9]. Thus, clarifying the molecular pathways that contribute to glioma advancement is essential, and novel approaches to treating gliomas are needed.

Tumor metastasis and malignant transformation are influenced by cell death [10–13]. Stockwell et al. discovered ferroptosis as a new mode of regulated cell death (RCD) [14]. The physical, metabolic, and genetic features of ferroptosis set it apart from other cell death modes. Ferroptosis is typically characterized by aberrant mitochondria (small size and condensed membrane), iron-dependent deadly lipid peroxide buildup, and a number of altered gene expressions, including GPX4, FSP1, AIFM2, and others [15–17]. A variety of ferroptosis-targeted reagents, such as ferroptosis inhibitors (for example, liproxstatin-1 and ferrostatin-1), as well as ferroptosis-inducing substances, have been discovered (eg, RSL3, erastin) [18]. In gliomas, glioma cells have a higher demand for reactive oxygen species (ROS) and iron metabolism than normal glial cells, rendering them more susceptible to ferroptosis [19]. Previous research has found that ferroptosis promotes the peroxidation of polyunsaturated fatty acids in membrane phospholipids by regulating the ACSL4 gene, leading to damage to the cell membrane and cell death [20,21]. Moreover, alterations in the expression of iron metabolism-related genes in glioma cells (DMT1, COPZ1, STEAP, etc.) can increase the iron content within these cells, thereby inducing ferroptosis [22–24]. The above studies demonstrate the immense potential of ferroptosis in the treatment of gliomas.

SMG9, a 520-amino acid protein with centrally located nucleotide triphosphatase domains, enhances GPX4 disintegration during ferroptosis in response to RSL3, a GPX4 inhibitor [25]. Elevated SMG9 expression levels have been correlated with poor prognosis in hepatocellular carcinoma (HCC), suggesting its potential as a treatment target [26]. However, its utility as a biomarker for glioma and its involvement in gliomas remain unclear. In this study, we utilized data from CGGA, TCGA, GTEX, and GEO databases to identify fourteen ferroptosis-associated biomarkers in glioma patients using machine learning techniques. SMG9, among the potential biomarkers, was selected for further investigation. The infiltration status of immune cells and its association with SMG9 in gliomas were examined using ssGSEA analysis. Additionally, expression pattern clustering and functional analysis of SMG9 were performed using Mfuzz. This research contributes to our understanding of the roles and processes of SMG9 in glioma.

2. Materials & methods

2.1. Data sources

The UCSC Xena Browser (https://xena.ucsc.edu/) was searched to retrieve RNA-Seq data from the TCGA database for 698 glioma samples and the GTEx database for 1157 samples of normal brain tissue. Additionally, the clinical data along with the mRNA-seq results of 1018 glioma samples were obtained from CGGA (http://cgga.org.cn/) [27]. Overall, this research included data from 749 samples with complete clinical records. Moreover, the GEO database (https://www.ncbi.nlm.nih.gov/geo/) was also searched for single-cell RNA-seq data from patients with glioma (accession number GSE202096). Meanwhile, 564 FRGs—including suppressors, drivers, unclassified, and markers—were extracted from the FerrDb database (http://zhounan.org/ferrdb) [28]. All procedures were accomplished with the aid of the Strawberry Perl (v. 5.32.1) and R (v. 4.2.2) programs.

2.2. Discovery of ferroptosis-related genes with differential expression

With the aid of the "limma" R package, the batch effect between the TCGA and GTEx was eliminated. After that, the "limma" package was also employed to search for DEGs between normal brain samples and glioma samples from the TCGA and GTEx datasets as per the following screening criteria: $|\log 2$ fold-change (FC)$| > 1$ and $P < 0.05$. Afterward, the DEGs associated with ferroptosis were found by taking the DEG list and the FRGs list and intersecting them to determine the overlapping genes. Furthermore, to investigate the protein-protein interaction (PPI) network of FRGs, we utilized the STRING database. The central genes were identified using the Maximal Clique Centrality (MCC) algorithms, which are part of the cytoHubba plug-in in Cytoscape (v3.7.2). We highlighted the most significant 20 genes as these core genes.

2.3. Glioma biomarker detection using machine learning methods

In this particular investigation, we made use of two different machine-learning techniques. To begin, the "randomForest" program was adopted to conduct the random forest analysis, after which only the most significant genes were selected. Following that, the LASSO regression analysis was done with the help of the "glmnet" package. The genes that were found to be present in both sets of results were regarded as candidates for use as biological markers in patients diagnosed with glioma.

2.4. Correlation and immune infiltration analyses of candidate biomarkers

The "corrplot" and "PerformanceAnalytics" packages were utilized to examine the correlation between possible biomarkers expression. The ssGSEA and CIBERSORT methods were applied to examine the degree to which TIICs (tumor-infiltrating immune cells)

are associated with gene expression patterns in tumor tissues. The ssGSEA method was employed to determine the relative infiltrating rates of the TCGA dataset's 24 different types of immune cells. The estimated Spearman correlations of the infiltration levels of 24 different immune cells with hub genes were displayed utilizing the ggplot 2 program. The CIBERSORT approach adopts a vector regression model in the process of cell type formation. As a result of its reliability, CIBERSORT might be applied to assess the impact of cell heterogeneity on the expression patterns of genes in complex tissues. After being used on the LM22-signed matrix, the algorism was further used to import the standard annotations of the gene expression data to the CIBERSORT platform. The acquired data were analyzed for associations of gene expression with the infiltration of immune cells.

2.5. Gene Ontology (GO) and Kyoto Encyclopedia of Genes and Genomes (KEGG) enrichment analyses of potential biomarkers

With the aid of the "clusterProfiler" program, we conducted GO and KEGG enrichment analyses on candidate biological markers, with a P-value of <0.05 serving as a scanning criterion for functional analysis. We next performed GO analysis to determine the specific cellular components (CCs), molecular functions (MFs), and biological processes (BPs) associated with the hub genes. Additionally, a KEGG enrichment analysis was done to determine the signaling pathways that were enriched by the candidate targets.

2.6. Gene set enrichment analysis (GSEA)

GSEA was used to investigate and clarify the reasons for observed fluctuations in the levels of candidate biomarkers in their coordinate pathways. Firstly, we obtained the GSEA program by downloading it from http://software. http://broadinstitute.org/gsea/index.jsp. Next, the c5.all.v7.2.symbols.gmt [Gene ontology] obtained from the Molecular Signatures Database (https://www.gsea-msigdb.org/) were employed as reference datasets. Finally, GSEA analysis and visualization were accomplished using "clusterProfiler" and "ggpolt2″ packages. The specified threshold value (P.adj <0.05) was used to determine the significance of enrichment in GSEA.

2.7. Single-cell analysis

The GEO database was searched to acquire the GSE202096 expression matrices. The "Seurat" program was used to conduct quality assurance and dimensionality reduction. In the first round of quality control, we generated Seurat objects for each of the glioma groups and then eliminated the cells expressing less than 200 genes. Genes expressing less than three cells were also excluded from the analysis. After that, normalization of gene expression patterns was done in the remaining cells, and the vst approach was used to identify 2000 high-variability genes within each sample. Following the scalarization of all genes, we conducted principal component analysis (PCA). Unsupervised clustering (resolution = 0.8) was used to cluster the cells, and the 20 leading principal components were then used to create a visual representation of the data in UMAP. The "singleR" package was utilized to annotate various cell types. The irGSEA was employed to undertake the merging of all of the single-cell rank-based GSEAs with the AVPs, and the UCell computation technique was used for the enrichment scoring approach.

2.8. Clustering of Mfuzz expression patterns and functional evaluation of optimum diagnostic markers

To determine which genes would provide the optimum diagnostic biological markers, we clustered Mfuzz expression profiles utilizing the "Mfuzz" package. Then, we computed the ssGSEA scores of several clustering modules, along with those of the glioma, and compared these scores to the expression characteristics with the normal group. After that, we determined the degree of correlation that existed between the clustering module and the biomarker, and afterward, we identified the gene module that was most strongly linked to the biomarker. After collecting gene modules, we conducted GO, KEGG, and GSEA to study and understand more about the gene functions of these modules.

2.9. Statistical analysis

R software was employed to conduct all analyses of statistical data. The "survminer" R program was used to produce Kaplan–Meier (KM) curves, and log-rank tests were implemented to derive P-values. To assess the factors associated with the overall survival (OS) of glioma patients, we conducted a univariate Cox regression analysis. To evaluate the predictive performance of SMG9, we generated a receiver operating characteristic (ROC) curve and computed the area under the curve (AUC).

2.10. Cell culture and transient transfection

The human glioma cell lines T98G, U87, and U251 as well as the normal human astrocytes HA were provided by Beijing Bena Biotechnology Institute and grown in F12 and DMEM containing 10% fetal bovine serum. Both cell lines were maintained in a humid incubator at 37 °C and 5% CO2. The negative control (NC) and SMG9 siRNA were transfected into the cells utilizing Lipofectamine 2000 (Invitrogen, USA). The target sequences for SMG9 siRNA were CTCCATCTTGACCTCCTTTTTCA (SMG9-si).

2.11. Western-Blot

RIPA buffer (Beyotime, China) was used to lyse the HA, T98G, U87, and U251 cell lines. The samples were then denatured at 100 °C for 15 min. Following a 10% SDS-PAGE separation, the protein samples were transferred to polyvinylidene fluoride (PVDF) membranes. After blocking with 5% BSA solution for an hour, primary antibodies, anti-SMG9 antibody (1:500, Proteintech, 24797-1-AP), anti-Nrf2 antibody (1:500, Proteintech, 80593-1-RR), anti-GPX4 antibody (1:500, Proteintech, 67763-1-Igˈ), anti-STAT1 antibody (1:500, Proteintech, 10144-2-AP), anti-P-STAT1 antibody (1:500, Proteintech, 28977-1-AP) and anti-GAPDH antibody (1:1000, Proteintech, 60004-1-Ig) were incubated on the membranes overnight. Then, secondary antibodies were applied for an additional 2 h at room temperature.

2.12. Quantitative RT-PCR

U87 and U251 cell lines total RNA was extracted using the TRIzol reagent (ThermoFisher, USA). Then, using the RNA from each sample, a quantitative reverse transcription-polymerase chain reaction was performed using SYBR Green Master (Roche, USA) and the Roche LightCycler 480 PCR System (2 μg). In a 20 μl reaction volume, the cDNA was utilized as a template along with 10 μl of PCR mixture, 0.5 μl of forward and reverse primers, 2 μl of cDNA template, and the necessary amount of water. PCR reactions were performed as follows: cycling conditions started with an initial DNA denaturation step at 95 °C for 30 s, followed by 45 cycles at 94 °C for 15 s, at 56 °C for 30 s, and at 72 °C for 20 s. Threshold cycle (CT) readings were collected and normalized to glyceraldehyde 3-phosphate dehydrogenase (GAPDH) levels in all samples using the $2^{-\Delta\Delta CT}$ method. The sequences of primer pairs for the target genes are shown below.

Gene	Forward primer sequence(5-3)	Reverse primer sequence(5-3)
SMG9	TCGGGAGAGGGACTACATTG	GTGGCTGTTTTGACCGCTC
IL-1β	AGCTACGAATCTCCGACCAC	CGTTATCCCATGTGTCGAAGAA
IL-6	ACTCACCTCTTCAGAACGAATTG	CCATCTTTGGAAGGTTCAGGTTG
IL-4	CGGCAACTTTGTCCACGGA	TCTGTTACGGTCAACTCGGTG
IL-10	TCAAGGCGCATGTGAACTCC	GATGTCAAACTCACTCATGGCT
CDH1	GCCTCCTGAAAAGAGAGTGGAAG	TGGCAGTGTCTCTCCAAATCCG
CDH2	CCTCCAGAGTTTACTGCCATGAC	GTAGGATCTCCGCCACTGATTC
VIM	AGGCAAAGCAGGAGTCCACTGA	ATCTGGCGTTCCAGGGACTCAT
GAPDH	AATGGGCAGCCGTTAGGAAA	GCCCAATACGACCAAATCAGAG

2.13. Cell viability

According to the manufacturer instructions, cell viability was determined using the Cell Counting Kit-8 test (Beyotime, China). In 96-well plates, cells from various treatments were grown at a density of 1×10^3 cells per well. The CCK-8 solution was used at the specified time intervals. Utilizing a microplate reader, the O.D 450 values of each well were determined during a 2-h incubation at 37 °C. (Thermo Fisher, USA).

2.14. Immunofluorescence detection

Cells were fixed with 4% paraformaldehyde at room temperature for 30 min and then treated with 0.4% Triton X-100 for 10 min and blocked with 2% bovine serum albumin for 30 min. The samples were cleaned with PBS, then treated with primary anti-E-cadherin antibodies (1:100, Proteintech, 20874-1-AP), anti-N-cadherin antibodies (1:100, Proteintech, 22018-1-AP) and anti-vimentin antibodies (1:100, Proteintech, 10366-1-AP), overnight at 4 °C. After that, they were exposed for an hour to the appropriate protein secondary antibodies. After three PBS washes and DAPI staining for 10 min, the slides were put under a fluorescence microscope.

2.15. Transwell assay

Transwell assays for invasion of U87 and U251 cell lines were performed. To test for migration and invasion, cells (5×10^4) were implanted into chambers covered with Matrigel (BD Biosciences, CA). In the upper layer, serum-free medium was supplied, and in the lower layer, full DMEM medium. Migrating or invading cells were fixed with 4% paraformaldehyde and stained with 0.1% crystalline violet following a 24-h incubation period. counting while using a flashlight.

2.16. Calcein AM/PI cytotoxicity assay

U87 and U251 cell lines were inoculated on cell crawls and washed with PBS. The Calcein AM/PI assay solution was added in an appropriate volume and incubated at 37 °C for 2 h. After incubation, the staining effect was observed under a fluorescent microscope protected from light.

2.17. Flow cytometry

In accordance with the manufacturer instructions, flow cytometry was used to examine the distribution of cell apoptosis. For cell apoptosis detection, cells were harvested with trypsin, followed by resuspending in PBS at the concentration of 1×10^5/200 μL. Cells were then stained for 30 min on ice with Annexin V-FITC and PI solution while being shielded from light. Samples were identified using a BD FACS Calibur flow cytometer (BD, USA) after being washed with PBS.

2.18. Measurement of intracellular ROS levels

With the aid of a Reactive Oxygen Species Assay Kit (Beyotime, China), the intracellular ROS levels were assessed. Briefly, after receiving various treatments, the cell pellets were collected and then resuspended in 1 ml of chilled PBS. DCFH-DA probe solution was treated with cells at 37 °C for 30 min in the dark. Every 5 min, the tube was turned over to mix the cells and solution. Using a BD FACS

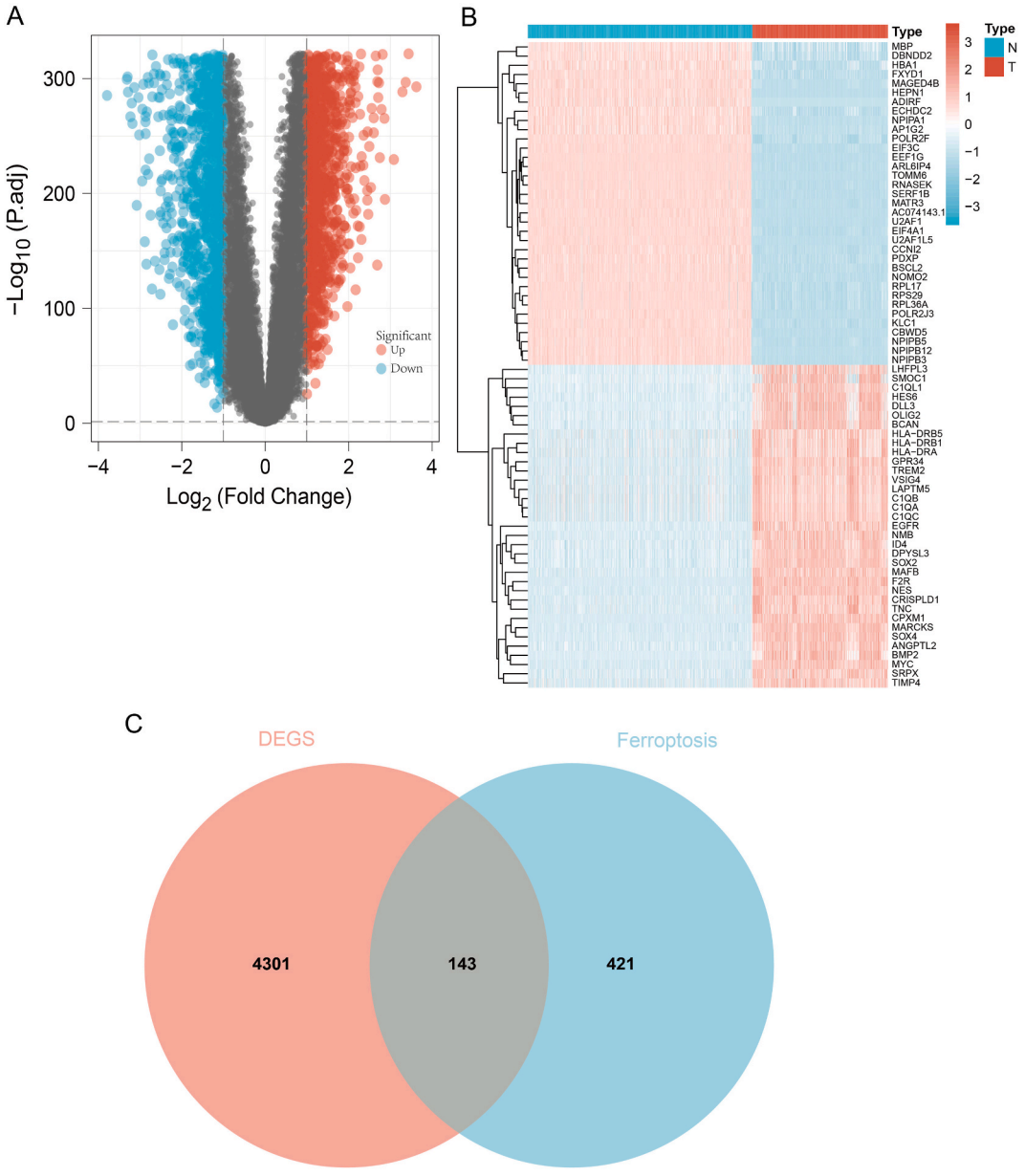

Fig. 1. The TCGA and GTEx database was searched for DEGs associated with ferroptosis. **(A)** Expression characteristics of DEGs, as shown by a volcano plot. **(B)** Expression of the top 35 DEGs in the dataset presented as a heat map. **(C)** A Venn diagram showing the overlap between DEGs and FRGs.

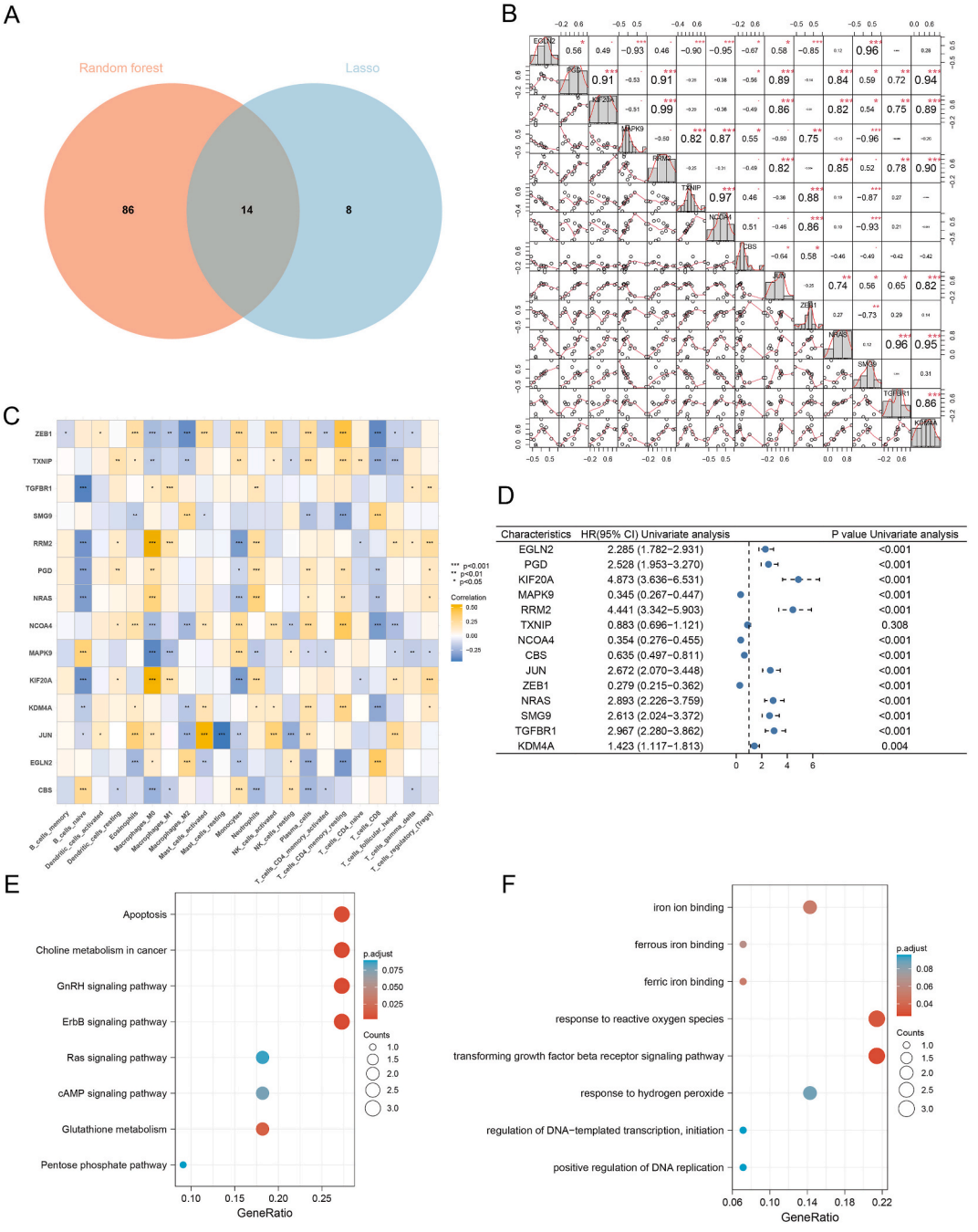

Fig. 2. **(A)** The Venn diagram of the potential biomarkers. **(B)** Correlation analysis between potential biomarkers. **(C)** The link between possible biomarkers and immune cell infiltration. **(D)** Univariate Cox regression analysis of 14 potential biomarkers associated with clinical prognosis in glioma. **(E)** Extensive investigation of 14 potential biomarkers using GO enrichment analysis. **(F)** Fourteen potential biomarkers were investigated by KEGG enrichment analysis.

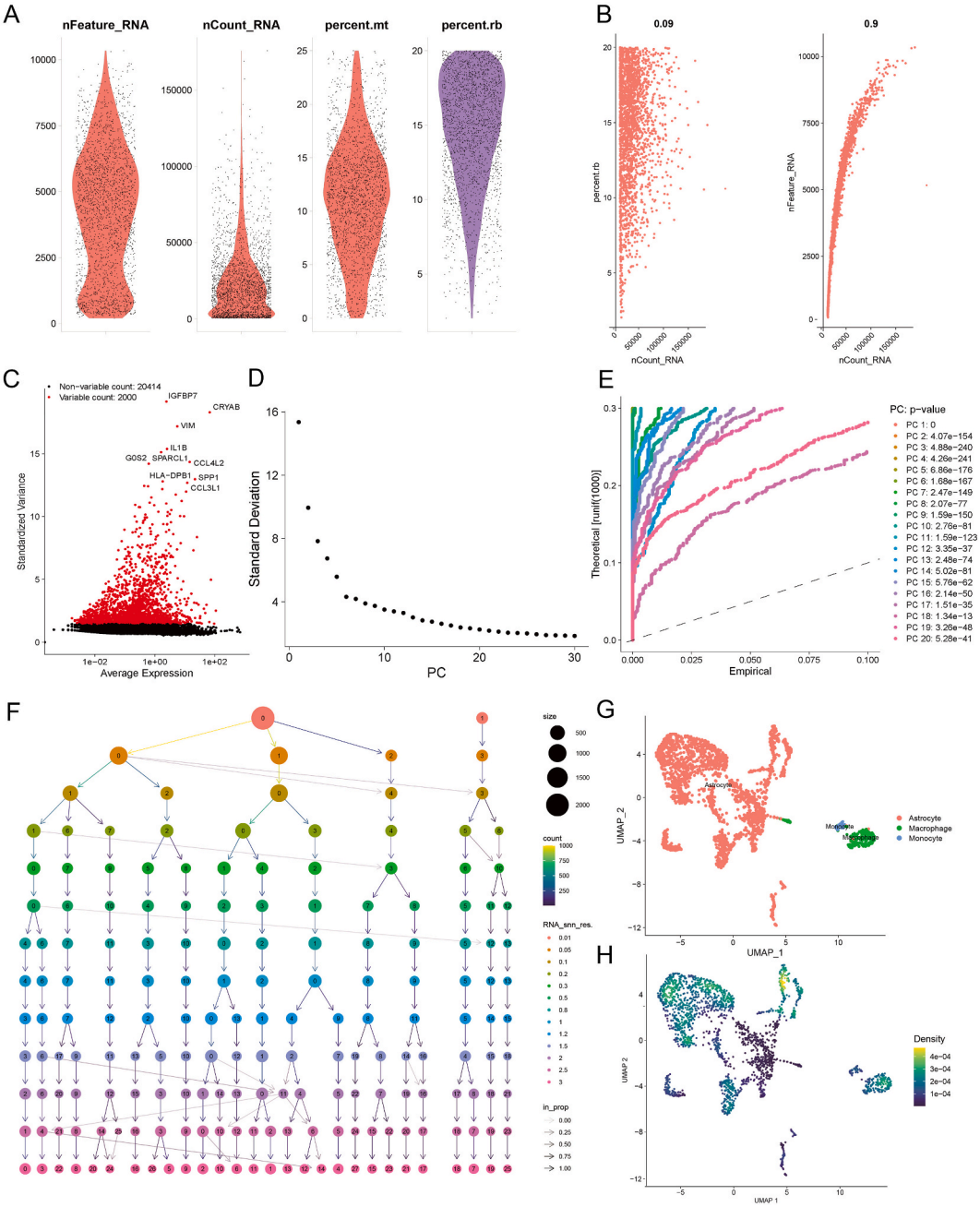

Fig. 3. Processing of scRNA-seq data. **(A)** Quality control of scRNA-seq data of glioma cell samples. **(B)** There was a favorable correlation between sequencing depth and the total number of identified genes. **(C)** Scatter diagrams illustrating the 2000 most significant DEGs **(D, E)** Cells were classified using principal component analysis, and the 20 leading PCs are presented. **(F)** clustertree was used to select the appropriate resolution. **(G)** Clustering analysis and visualization of glioma single-cell transcriptomic data using UMAP. The overall identification of each cell cluster is depicted on the right and is denoted by the color assigned to each cluster. **(H)** Fourteen potential biomarkers are shown in a density scatterplot as a set of genes.

Calibur flow cytometer (BD, USA), samples were cleaned three times with serum-free media before being measured at 488 nm excitation and 525 nm emission.

3. Results

3.1. Discovery of differentially expressed genes in glioma patients

From TCGA and GTEX databases, 4444 DEGs were acquired in the glioma patients; of these DEGs, 2216 were upregulated, whereas 2228 were downregulated (Fig. 1A–B). Fig. 1B displays the 35 leading DEGs with significant differences in terms of expression between glioma and normal controls. After intersecting the DEGs and the FRGs, 143 FRGs were found to be differentially expressed (Fig. 1C).

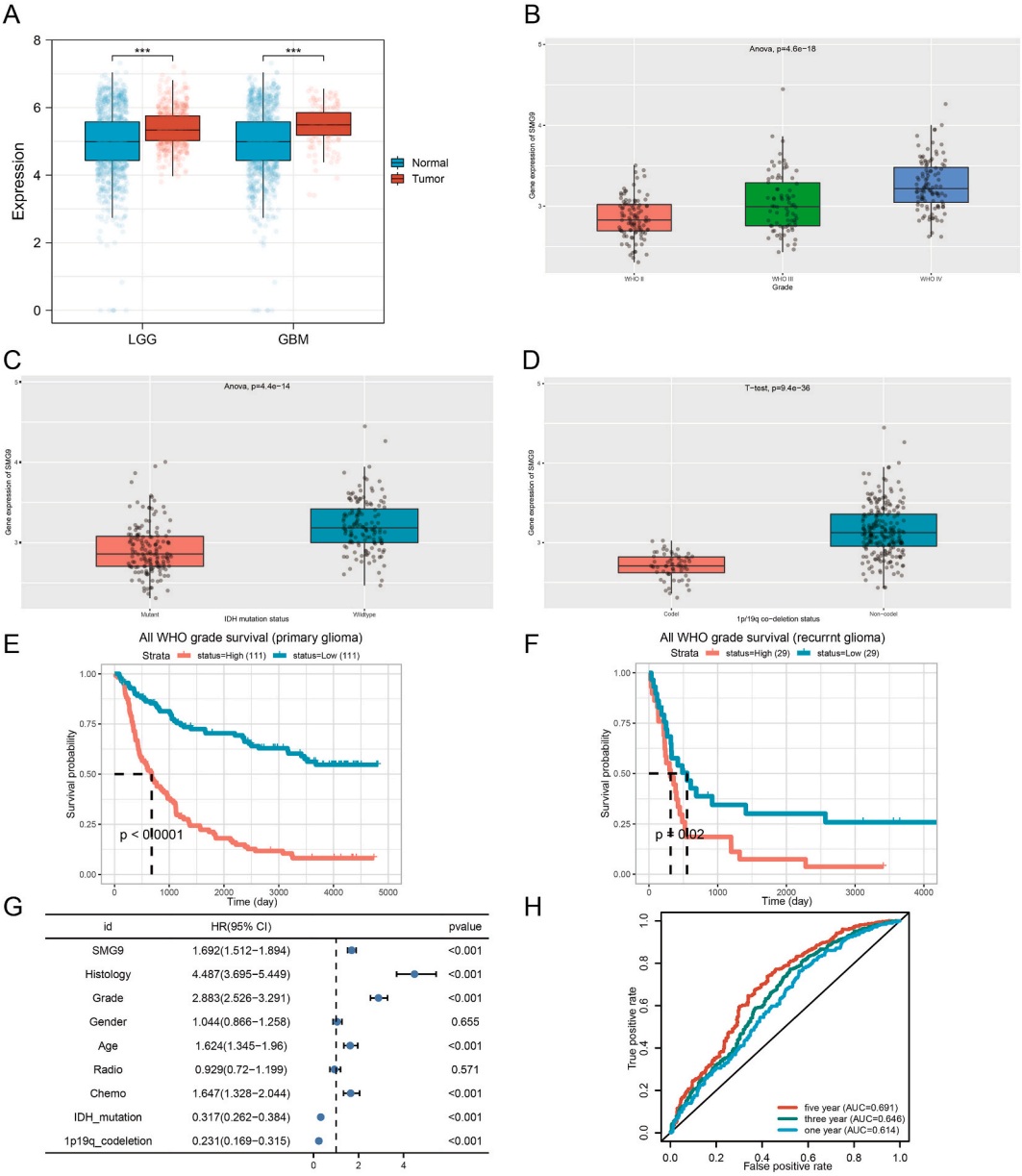

Fig. 4. **(A)** In TCGA, SMG9 expression considerably varies between GBM and LGG. SMG9 expression in CGGA **(B)** WHO grades. **(C)** IDH status-stratified distribution. (D) 1p/19q-codeletion status distribution. SMG9 expression in glioma patients, as shown by the Kaplan-Meier survival plot **(E)** Dataset ID: mRNAseq_325-Primary Glioma **(F)** Dataset ID: mRNAseq_325-recurrent Glioma. **(G)** Clinical and pathological factors, including SMG9 expression, obtained from the CGGA dataset **(H)** Survival rates for 1-, 3-, and 5- year periods as depicted by time-depending receiver operating characteristic (ROC) curves.

Furthermore, the hub gene of FRGs was identified (Fig. S1)

3.2. Ferroptosis-related biomarkers screening in patients with glioma by machine learning methods

In this work, we applied machine learning methods to delve further into the possible biological markers in 143 primary targets for ferroptosis-related glioma. The findings of the random forest were used to select the 100 leading genes as possible biological markers (Figs. S2A and B). Moreover, glioma patients' prognoses were integrated to develop the LASSO regression model. The λ analysis revealed that the model provided reliable prognostic predictions when $\lambda = 22$. Accordingly, 22 candidate genes were found using LASSO analysis (Figs. S2C and D). Lastly, the findings derived from the two algorithms were integrated and yielded EGLN2, PGD, KIF20A, MAPK9, RRM2, TXNIP, NCOA4, CBS, JUN, ZEB1, NRAS, SMG9, TGFBR1 and KDM4A as ferroptosis-related glioma potential biomarkers (Fig. 2A).

3.3. Correlation between candidate biological markers and immune cell infiltration analyses

The initial results of the correlation study demonstrated a remarkably positive relationship between SMG9 and the expression of EGLN2 in glioma patients. The expression patterns of MAPK9, TXNIP, and NCOA4 all correlated negatively with SMG9 (Fig. 2B). Subsequently, we performed CIBERSORT immune infiltration analyses of the fourteen potential biomarkers. The relationship between candidate biological markers and 22 kinds of immune cells is shown in the heatmap (Fig. 2C). Meanwhile, the univariate Cox analysis of fourteen potential biomarkers showed that 9 genes were risk factors with HR > 1 for glioma prognosis (Fig. 2D).

3.4. Pathway enrichment analysis of potential biomarkers

We conducted a pathway enrichment analysis to delve deeper into the biological roles of the candidate biomarkers. The findings of the GO enrichment analysis illustrated that the majority of the candidate biological markers were associated with the processes of apoptosis, choline metabolism in cancer, and the GnRH signaling pathway (Fig. 2E). As per the outcomes of the KEGG enrichment analysis, prospective biomarkers were mostly linked to the transforming growth factor beta (TGF-β) receptor signaling pathway, the

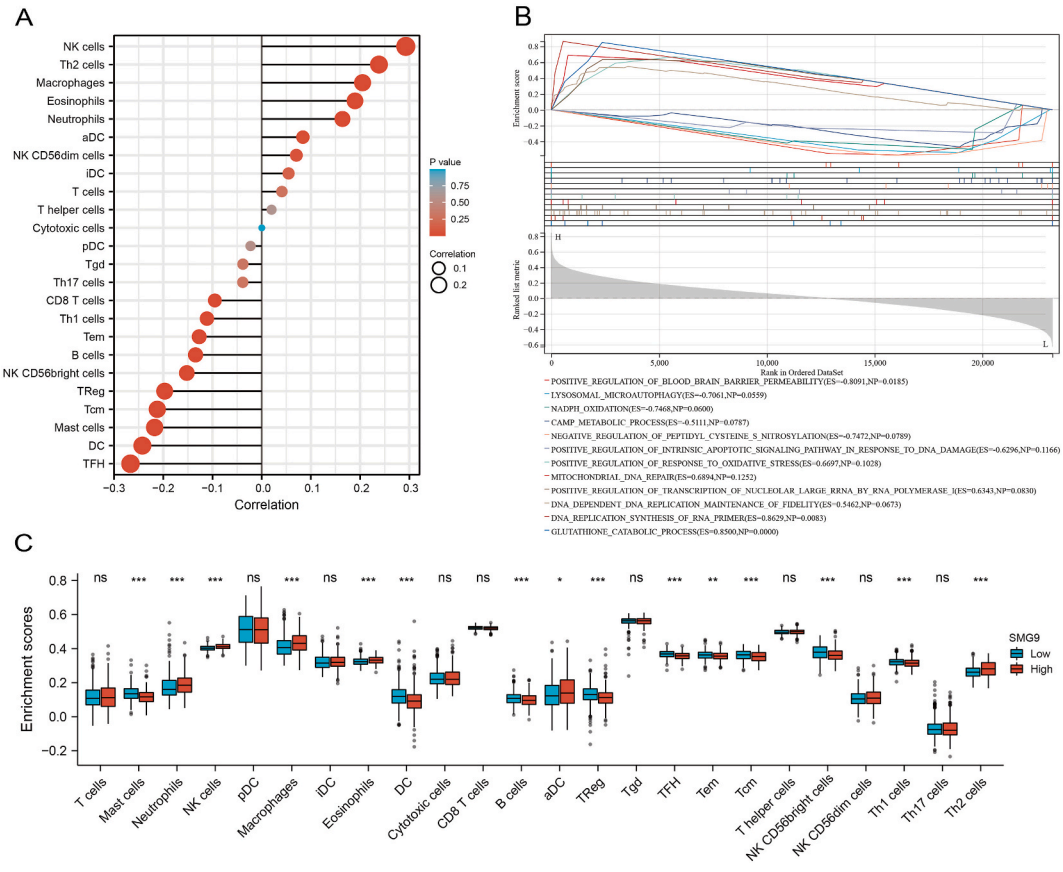

Fig. 5. **(A)** The association of SMG9 with immune cell infiltration in glioma. **(B)** GSEA analysis of SMG9. **(C)** Relative TIIC ratios calculated by the ssGSEA technique with data from the TCGA.

response to reactive oxygen species, and the iron ion binding pathway (Fig. 2F).

3.5. Single-cell level transcriptomic landscape of potential biomarkers

Quality assurance identified 22,414 genes within 2341 cells. Vlnplots were used to present information on the number of genes (nFeature), the proportion of ribosomal genes (percent.rb), the proportion of mitochondrial genes (percent.mt), and the sequence count per cell (nCount) (Fig. 3A). As per the findings of the correlation analysis, nCount had a positive link to nFeature (Fig. 3B). After that, a scatter diagram was constructed using the data from 2000 variable genes (Fig. 3C). It was found that there was a significant level of heterogeneity in the glioma cells, as shown by the discovery of thirty principal components (PCs) (Fig. 3D–E). Meanwhile, clustertree was used to select the appropriate resolution (Fig. 3F). The UMAP analyses were conducted on the top-ranked twenty PCs in the matrix. Glioma cells, as determined by UMAP and cell-type annotation, were grouped into three distinct categories: Astrocyte, Macrophage, and Monocyte (Fig. 3G). Fig. S3 depicts the expression patterns of fourteen potential biomarkers in the glioma cell populations Furthermore, single-cell GSEA (scGSEA) demonstrated that astrocytes and macrophages had a higher enrichment score than other cell types (Fig. 3H).

3.6. The association of SMG9 expression with WHO grade and IDH1 phenotype in glioma

The role of SMG9 in glioma has not been previously reported. We selected SMG9 from 14 potential biomarkers for a follow-up study. The SMG9 expression level was elevated in both LGG (num (N) = 1152, num (T) = 529) and GBM (num (N) = 1157, num (T) = 169). In particular, SMG9 was expressed at a high level in malignant tissues (Fig. 4A). Moreover, the CGGA datasets were examined for links between SMG9 expression and WHO grade and IDH1 status. Consequently, severe malignancy in gliomas was

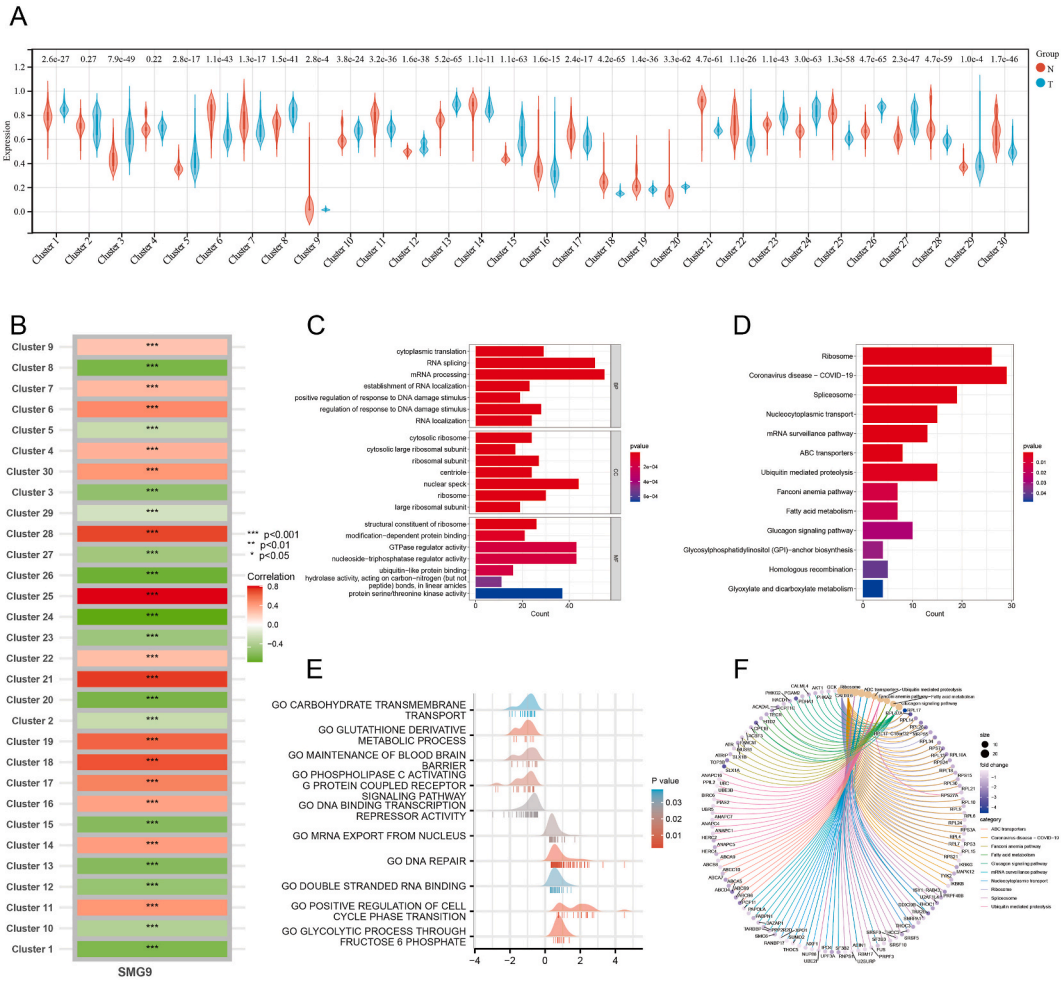

Fig. 6. **(A)** The tumor (T) and normal (N) groups were compared by their ssGSEA scores of clustering modules and expression features. **(B)** Link between the clustering module and SMG9. **(C)** Functional enrichment analysis of the genes in the Cluster25 module based on GO terms. **(D, E)** The KEGG functional enrichment results of Cluster25 module genes. **(F)** The GSEA analysis results of Cluster25 module genes.

associated with enhanced SMG9 expression (Fig. 4B). Finally, the IDH-wildtype group had remarkably elevated SMG9 levels in contrast with the IDH-mutant group (Fig. 4C). We found a considerable enhancement in SMG9 expression in the 1p/19q-non-codeletion (non-codel) group in contrast with the 1p/19q-codeletion (codel) group (Fig. 4D), as determined via the ANOVA test. These results demonstrated that SMG9 was highly expressed in the IDH-wildtype and 1p19q-non-codeletion groups.

3.7. Independent predictive value of SMG9 in patients with glioma

SMG9 overexpression was an indicator of a more adverse OS in primary and recurrent glioma, as per the survival analysis that was performed based on the CGGA databases (Fig. 4E–F). In addition, to evaluate the utility or practicality of SMG9 expression, we conducted a univariate Cox analysis. The findings discovered various factors including SMG9 expression ($P < 0.001$), 1p19qcodeletion

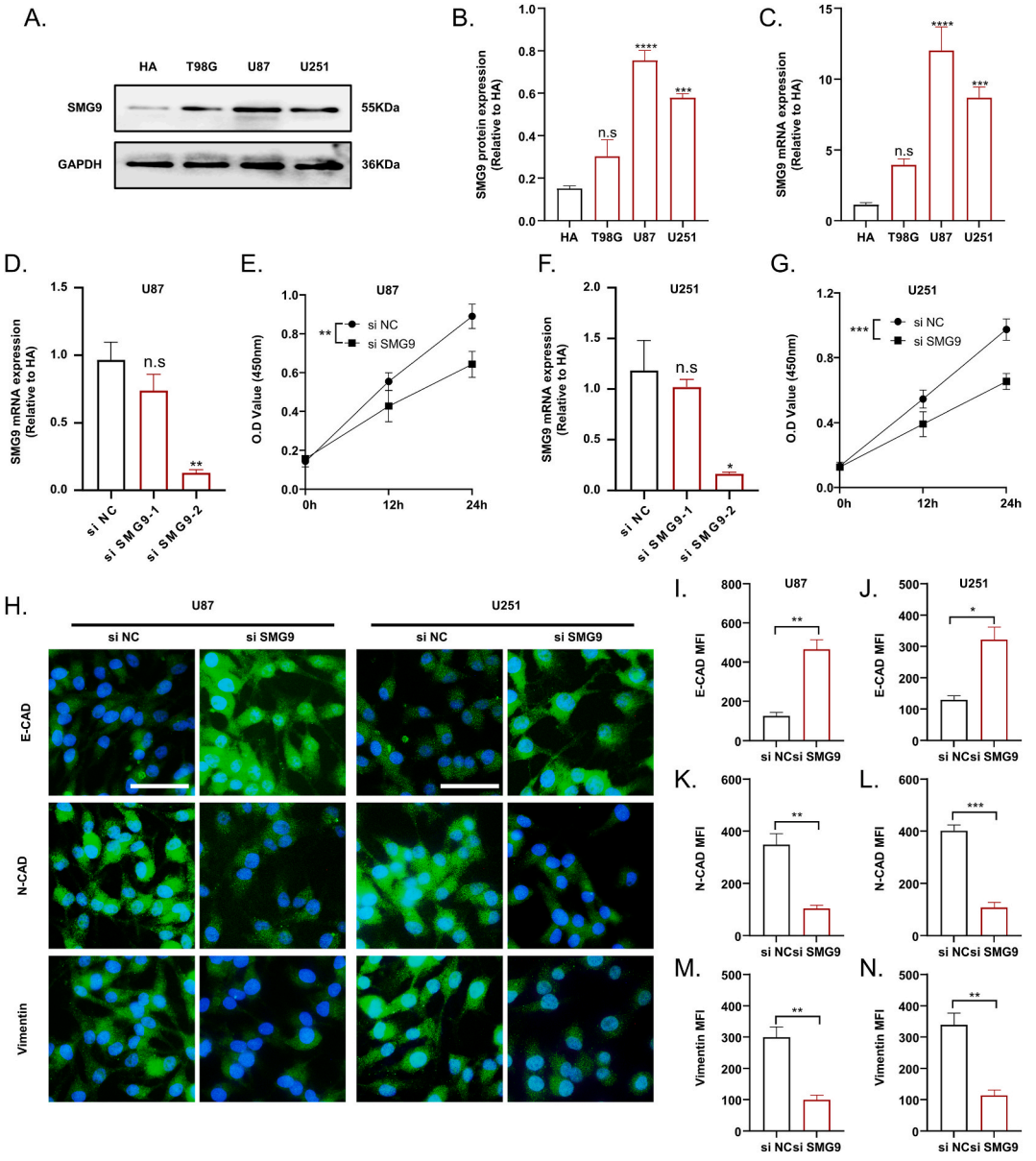

Fig. 7. (A–B) Protein expression of SMG9 in human astrocytes HA and glioma cell lines T98G, U87 and U251 and its quantitative analysis. **(C)** Expression of SMG9 mRNA in human astrocytes HA and glioma cell lines T98G, U87 and U251 and its quantitative analysis. **(D–E)** The infection efficiency of si SMG9 and the results of CCK8 after inhibition of SMG9 were examined in U87 cell line. **(F–G)** The infection efficiency of si SMG9 and the results of CCK8 after inhibition of SMG9 were examined in U251 cell line. **(H)** Representative immunofluorescence results of E-CAD, N-CAD and vimentin after inhibition of SMG9 in U87 and U251 cell lines. **(I–N)** Quantitative analysis of the mean fluorescence intensity against E-CAD, N-CAD and vimentin. N = 3, *≤0.05, **≤0.01 , ***≤0.001 , ****≤0.0001. The results are presented as mean ± S.E.M.

(P < 0.001), IDH mutation (P < 0.001), chemotherapy (P < 0.001), grade (WHO grade) (P < 0.001), and histology (P < 0.05) (Fig. 4G). The ROC analysis showed that the AUC values of SMG9 in predicting 1-, 3-, and 5-year survival were 0.614, 0.646, and 0.691, correspondingly (Fig. 4H).

3.8. Immune infiltration analyses and GSEA of SMG9

In this study, we analyzed the association of TIICs with SMG9 expression profiles in glioma. Our data confirmed that SMG9 expression was positively linked to many different types of immune cells, including NK cells, Th2 cells, Macrophages, Eosinophils, Neutrophils, aDC, and T cells (Fig. 5A). The 703 TCGA samples were classified into low- and high- SMG9 expression categories to confirm the association of TIICs in glioma with SMG9. It was found that the high-risk category had a relatively low level of immune cell infiltration (Mast cells, DC cells, B cells, TReg, TFH, Tcm, and Th1 cells) in contrast with the low-risk category. Moreover, the infiltration levels of Neutrophils cells, NK cells, Macrophages, Eosinophils, and Th2 cells were remarkably elevated in the high-risk

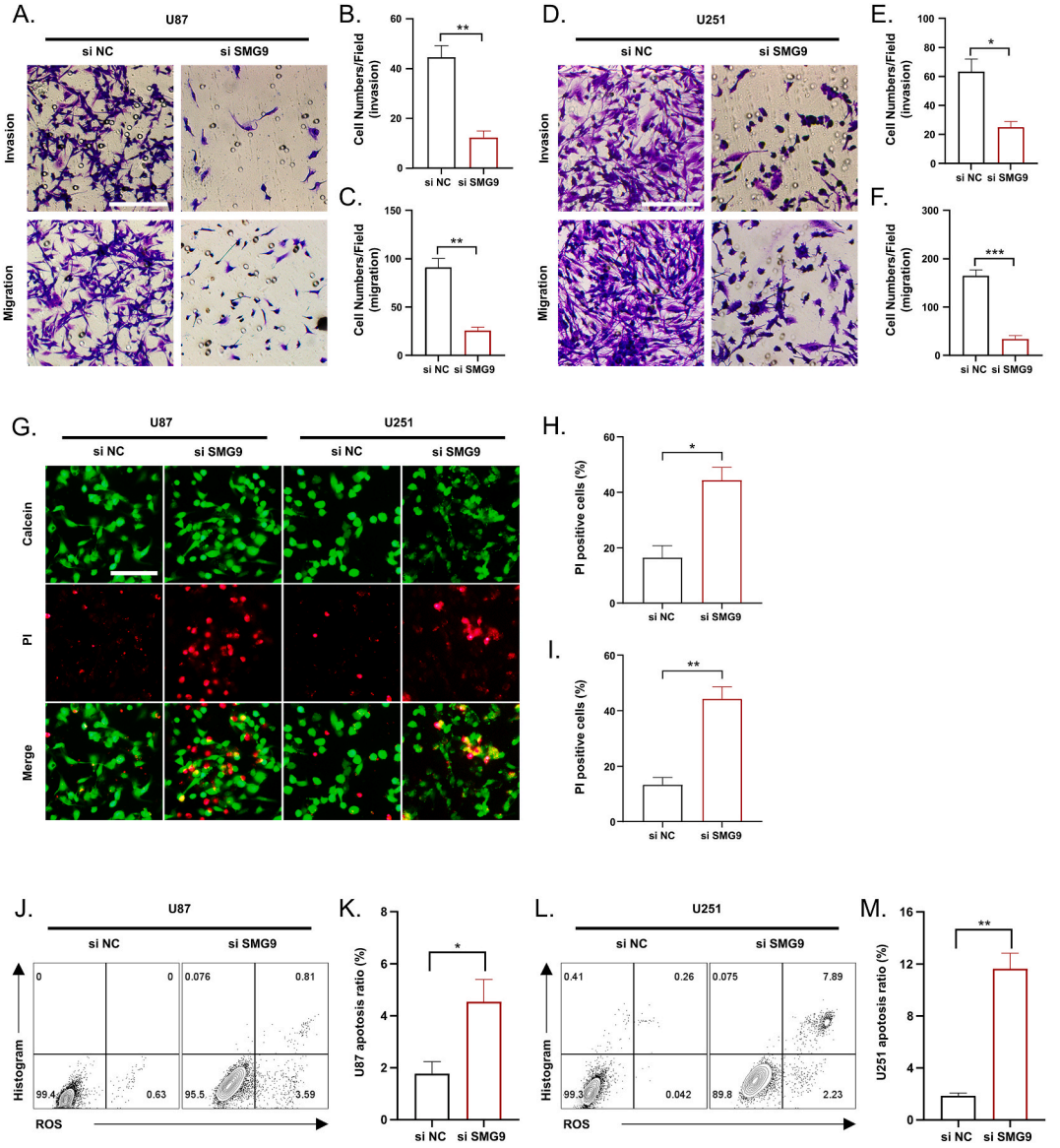

Fig. 8. **(A–C)** Representative migration as well as invasive ability of U87 cell line after inhibition of SMG9 and quantification of cell numbers. **(D–F)** Representative migration as well as invasive ability of U251 cell line after inhibition of SMG9 and quantification of cell numbers. **(G–I)** Representative live-dead cell staining results of U87 and U251 cell lines after SMG9 inhibition and quantitative analysis. **(J–M)** Representative apoptosis results of U87 and U251 cell lines after SMG9 inhibition and quantitative analysis. N = 3, *≤0.05, **≤0.01 , ***≤0.001 , ****≤0.0001. The results are presented as mean ± S.E.M.

category relative to the low-risk category (Fig. 5C). To investigate the possible biological function of SMG9, we conducted a GSEA. We found that the expression of SMG9 was highly associated with twelve different gene pathways. In addition, SMG9 had a remarkable link to gene pathways that were related to damage (Fig. 5B).

3.9. Clustering of Mfuzz expression pattern and functional analysis of SMG9

We acquired a total of thirty different clustering findings after clustering the Mfuzz expression pattern into clusters according to the level of SMG9 expression (Fig. S4). These findings, together with the expression features and the clustering module's ssGSEA score, led to the discovery of clustering between the glioma samples and the normal controls (Fig. 6A). We also discovered a link between SMG9 and the class modules (Fig. 6B). Enrichment analysis of genes in the Cluster25 module revealed that they are involved in the modulation of DNA damage response, RNA biological process, glutathione metabolism, and blood-brain barrier, in the SMG9 enrichment functions. In addition, we also discovered glycolysis and ribosome correlative signaling pathways, and this may aid in understanding SMG9-related possible mechanisms (Fig. 6C–F).

3.10. SMG9 promotes the development of glioma

To verify the reliability of the bioinformatics results, we examined the expression of SMG9 in human astrocytes HA as well as glioma cell lines T98G, U87 and U251 by WB and PCR experiments. It could be observed that the expression of SMG9 was significantly higher in U87 and U251 cell lines than in HA. To clarify the role played by SMG9 in the development of glioma (Fig. 7A–C). We

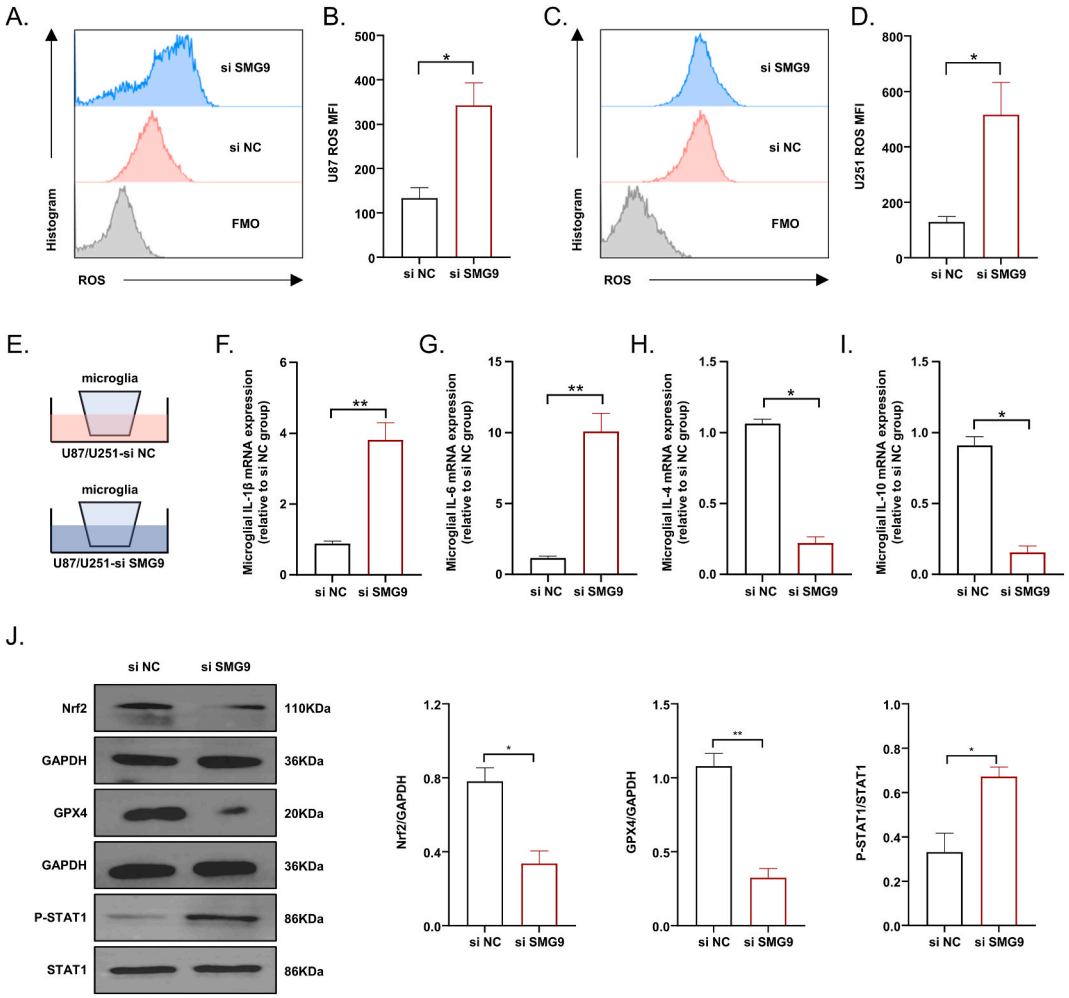

Fig. 9. **(A–D)** Representative ROS staining results of U87 and U251 cell lines after inhibition of SMG9 and quantification of the mean fluorescence intensity of ROS. **(E)** Schematic diagram of glioma cell lines co-cultured with microglia. **(F–I)** Expression of IL1β, IL6, IL4 and IL10 mRNA in microglia. **(J)** Representative WB results of Nrf2, GPX4 and phosphorylated STAT1 in glioma cell lines after inhibition of SMG9 and quantitative analysis. N = 3, *≤0.05, **≤0.01 , ***≤0.001 , ****≤0.0001. The results are presented as mean ± S.E.M.

constructed two small interfering RNAs against SMG9 and transferred them into U87 and U251 cell lines. The results of PCR showed that the interference effect of si SMG9-2 was better than that of si SMG9-1. After inhibiting SMG9 expression in U87 and U251, we examined the cell viability of U87 and U251 by CCK8. The results showed that the activity of glioma cell lines was significantly reduced after inhibition of SMG9 (Fig. 7D–G). Epithelial mesenchymal transition (EMT) plays an important role in the development of glioma. Inhibition of SMG9 resulted in decreased expression of N-CAD and vimentin and increased expression of epithelial maker-E-CAD in U87 and U251 cell lines (Fig. 7H–N, Fig. S5). Meanwhile, inhibition of SMG9 expression in U87 and U251 cell lines resulted in decreased migration as well as invasive ability of cells (Fig. 8A–I) and increased apoptosis (Fig. 8J–M).

3.11. SMG9 causes immunosuppression of glioma

ROS expression was increased in U87 and U251 cell lines after inhibition of SMG9 (Fig. 9A–D). The functional status of microglia, as important cells performing phagocytic and antigen-presenting functions in the central nervous system, is crucial for the treatment of gliomas. By transwell in vitro co-culture system, we co-cultured glioma cell lines and glioma cell lines that inhibit SMG9 expression with microglia. We found that inhibition of SMG9 expression in glioma cell lines resulted in increased expression of IL1β and IL6 in microglia, while IL4 and IL10 expression decreased (Fig. 9E–I). We also examined the expression of Nrf2, GPX4 and STAT1 in glioma cell lines after SMG9 inhibition. the expression of Nrf2 and GPX4 decreased after SMG9 inhibition while the expression of phosphorylated STAT1 increased (Fig. 9J).

4. Discussion

According to statistics, 12–15% of all intracranial tumors are glioblastoma multiforme (GBM), a primary neuroepithelial malignant neoplasm of the CNS [29–31]. There are around three individuals diagnosed with GBM for every 1000 persons, and the conventional duration a patient survives after being diagnosed with the disease is only about 12–18 months. The five-year survival rate is around 5.5%, whereas the ten-year survival rate is around 2.9% [32,33]. The lack of effective treatment targets may contribute to the dismal prognosis and short life expectancy of individuals with GBM. As a result, the identification of novel therapeutic targets is of the tmost importance.

In this research, we used machine learning techniques to select 14 possible ferroptosis-related biomarkers as candidates for further analyses. Additionally, their immune cell infiltration, clinical correlation, probable action mechanism, and expression in single cells were investigated and analyzed. The role of SMG9 in glioma has not been reported. We selected SMG9 from 14 potential biomarkers for a follow-up study. This work demonstrated the significance of SMG9 in the etiology of glioma, uncovered a novel prospective treatment target for glioma, and identified a marker of patient prognosis. Patients who were diagnosed with glioma had a poor chance of surviving the disease and an elevated level of SMG9. In addition, the correlations of SMG9 expression with IDH1 statuses were probed for this research. As indicated by the World Health Organization (WHO), IDH1 phenotypes are a unique diagnostic approach that is used in clinical settings [34–36]. Additionally, the status of an individual's IDH1 mutation is used in adults to categorize diffuse gliomas. The degree to which SMG9 is expressed in gliomas is linked to whether or not they have the IDH1 phenotype. Also, we conducted COX and ROC analyses to emphasize the importance of SMG9, and we discovered that SMG9 is a molecular marker that may be used to predict glioma patients' prognoses.

SMG9 is a participant in the nonsense-mediated decay (NMD) pathway, which binds directly to SMG1 and SMG8 to generate a complex composed of SMG1, SMG8, and SMG9 that is very stable [37,38]. SMG9 is an indispensable constituent of the NMD, hence it assumes an instrumental function in the NMD pathway. Evidence is mounting indicating the NMD pathway is engaged in a wide variety of biological activities, some of which include the immunological response and stress response [39,40]. The NMD may be disrupted, which can result in intellectual impairment as well as malignancy. Notably, The relationship between NMD and cancer is a complex one [41]. Interestingly, tumors exploit NMD to downregulate the expression of critical tumor-suppressor genes, while simultaneously modifying NMD activities to suit their microenvironment [42,43]. In a study by Jin et al., SMG9 was shown to be overexpressed in HCC tissues, and this was correlated with a worse prognosis for patients. SMG9 remarkably enhanced HCC cell line functioning, such as proliferation, cell cycle progression, apoptotic resistance, invasion, and migration. The epithelial–mesenchymal transition (EMT) and the Wnt/-catenin signaling pathway may be important in driving these processes [26]. In the previous study, SMG9, an element of the NMD mechanism, was shown to be a selective trigger for ferroptosis in human cancer cells. Aside from its role in NMD, SMG9 also favorably modulates ferroptosis. Also, in response to the GPX4 inhibitor but not the SLC7A11 inhibitor, SMG9 acts as a direct binding protein of GPX4 to induce its disintegration. GPX4 accumulates in the mitochondria after genetic suppression of SMG9, protecting them from oxidative stress, and promoting resistance to ferroptosis in the long run, either in xenograft mice models or in vitro. The results of this research suggest that SMG9 could be involved in other biological processes besides NMD [25]. Based on our findings and previous research on SMG9, it is reasonable to hypothesize that SMG9 participates in the progression of physiological and pathological pathways associated with glioma although the link between SMG9 and glioma is not yet fully understood.

The GSEA was conducted to analyze the candidate biological functions that SMG9 plays in glioma. As per the results of the GSEA, there were significant variations in the enrichment of pathways between samples containing low and high levels of SMG9. Specifically, GESA demonstrated enrichment of oxidation-associated and DNA damage repair gene sets, such as positive modulation of the oxidative stress response, positive modulation of the intrinsic apoptotic signaling pathway in response to DNA damage, and mitochondrial DNA repair. In addition, the probable role of SMG9 was investigated with the use of Mfuzz algorithms. Similar to the SMG9 enrichment function, the functional enrichment findings of Cluster25 module genes demonstrated that these genes are engaged in modulating the DNA damage repair response, RNA biological process, and the functioning of the blood-brain barrier (BBB). Notably, glioma

progression is linked to both DNA damage repair and BBB function. Based on these findings, SMG9 may play a role in glioma development. Our data suggest that SMG9 upregulation is associated with a dismal prognosis. We thus predict that SMG9 overexpression may assume an essential regulatory role in these carcinogenic pathways, leading to worse prognoses in glioma individuals.

Ferroptosis and immunity interplay, with ferroptosis impacting the tumor immune infiltration. We explored how SMG9 expression is associated with immune cell infiltration into gliomas. As per the findings of the ssGSEA, the SMG9 expression was shown to have a strong inverse relationship with the infiltration levels of DC cells, B cells, Mast cells, TReg, TFH, Tcm, and Th1 cells. DCs are robust antigen-presenting cells, and they perform fundamental functions in the modulation of T-cell immunity. Notably, DCs are becoming more popular in vaccination protocols because they enhance the immunogenicity of certain antigens in patients. Tumor-specific cytotoxic T cells and NK cell immunity may be stimulated by DCs. Because of their ability to stimulate T cells, DCs play a crucial part in the onset and progression of gliomas [44,45]. Mast cells are specialized cells of the immune system that secrete a broad variety of biologically active substances that may stimulate, dampen, or otherwise modulate immunity [46–48]. As a result, we hypothesized that SMG9 could affect tumor immunity.

Finally, by revealing their potential importance to the immune response to tumors, we found new FRGs with therapeutic use for glioma. Additionally, this is the first study demonstrating the involvement of SMG9 in glioma. Glioma individuals have an increased level of SMG9, which is also correlated with tumor grade. Moreover, upregulation of SMG9 in glioma is associated with a poor prognosis and attenuated immune cell infiltration. There were, however, certain limitations to the research. For example, neither in vitro nor in vivo testing was performed. Accordingly, further study is warranted to confirm SMG9's potential as a predictive biomarker in glioma.

Data availability statement

Data will be made available on request.

Funding

This study is supported by Nantong First People's Hospital Provincial and ministerial High level Science and Technology Project Cultivation Fund (YPYJJYB006), State Key Laboratory of Oncogenes and Related Genes Research Project (KF-2203-93), Nantong University Clinical Medicine Special Project (2022JY003, 2022LY009, 2022HY003), The first phase of "Research and Innovation Team Project" of Kangda College of Nanjing Medical University (KD2022KYCXTD006), TCM Science and Technology Development Plan of Jiangsu Province (MS2021060).

CRediT authorship contribution statement

Yong Dai: Writing – review & editing, Writing – original draft, Visualization, Validation, Supervision, Software, Resources, Project administration, Methodology, Investigation, Formal analysis, Data curation, Conceptualization. **Huan Zhang:** Writing – review & editing, Writing – original draft, Visualization, Data curation, Conceptualization. **Sujuan Feng:** Writing – review & editing, Methodology, Investigation, Formal analysis, Data curation. **Chao Guo:** Writing – review & editing, Resources, Methodology, Investigation, Formal analysis, Data curation, Conceptualization. **Wenjie Tian:** Writing – review & editing, Software, Methodology, Investigation, Formal analysis, Data curation. **Yimei Sun:** Writing – review & editing, Writing – original draft, Supervision, Resources, Project administration, Methodology, Investigation, Funding acquisition. **Yi Zhang:** Writing – review & editing, Writing – original draft, Supervision, Resources, Project administration, Funding acquisition, Data curation, Conceptualization.

Declaration of competing interest

The authors declare that they have no known competing financial interests or personal relationships that could have appeared to influence the work reported in this paper.

Appendix A. Supplementary data

Supplementary data to this article can be found online at https://doi.org/10.1016/j.heliyon.2024.e25716.

References

[1] A. Jemal, F. Bray, M.M. Center, J. Ferlay, E. Ward, D. Forman, Global cancer statistics, Ca - Cancer J. Clin. 61 (2) (Mar-Apr 2011) 69–90, https://doi.org/10.3322/caac.20107.

[2] X.Q. Ge, Z.H. Wang, R. Jiang, et al., SCAMP4 is a novel prognostic marker and correlated with the tumor progression and immune infiltration in glioma, Int. J. Biochem. Cell Biol. (2021) 139106054, https://doi.org/10.1016/j.biocel.2021.106054.

[3] S. Tanaka, D.N. Louis, W.T. Curry, T.T. Batchelor, J. Dietrich, Diagnostic and therapeutic avenues for glioblastoma: no longer a dead end? Nature reviews Clinical oncology. Jan 10 (1) (2013) 14–26, https://doi.org/10.1038/nrclinonc.2012.204.

[4] Y. Yan, Z. Xu, S. Dai, L. Qian, L. Sun, Z. Gong, Targeting autophagy to sensitive glioma to temozolomide treatment, J. Exp. Clin. Cancer Res. : CR 35 (2016) 23, https://doi.org/10.1186/s13046-016-0303-5.

[5] J. Ho, J. Ondos, H. Ning, et al., Chemoirradiation for glioblastoma multiforme: the national cancer institute experience, PLoS One 8 (8) (2013) e70745, https://doi.org/10.1371/journal.pone.0070745.

[6] J.G. Nicholson, H.A. Fine, Diffuse glioma heterogeneity and its therapeutic implications. Cancer discovery, Mar 11 (3) (2021) 575–590, https://doi.org/10.1158/2159-8290.Cd-20-1474.

[7] E.G. Van Meir, C.G. Hadjipanayis, A.D. Norden, H.K. Shu, P.Y. Wen, J.J. Olson, Exciting new advances in neuro-oncology: the avenue to a cure for malignant glioma, Ca - Cancer J. Clin. 60 (3) (2010) 166–193, https://doi.org/10.3322/caac.20069.

[8] K.Y. Yeung, A. Dickinson, J.F. Donoghue, et al., The identification of mitochondrial DNA variants in glioblastoma multiforme, Acta neuropathologica communications 2 (2014) 1, https://doi.org/10.1186/2051-5960-2-1.

[9] Z. Chen, X. Wei, L. Shen, H. Zhu, X. Zheng, 20(S)-ginsenoside-Rg3 reverses temozolomide resistance and restrains epithelial-mesenchymal transition progression in glioblastoma, Cancer Sci. 110 (1) (2019) 389–400, https://doi.org/10.1111/cas.13881.

[10] S.Y. Lee, M.K. Ju, H.M. Jeon, et al., Regulation of tumor progression by programmed necrosis, Oxid. Med. Cell. Longev. 2018 (2018) 3537471, https://doi.org/10.1155/2018/3537471.

[11] V. Labi, M. Erlacher, How cell death shapes cancer, Cell Death Dis. 6 (3) (2015) e1675, https://doi.org/10.1038/cddis.2015.20.

[12] X. Yang, J. Qu, J. Li, Nicotinic acid induces apoptosis of glioma cells via the calcium-dependent endoplasmic reticulum stress pathway, Biocell 46 (4) (2022) 1041.

[13] G. Xiang, J. Wenqu, Z. Guofeng, et al., AQP1 as a novel biomarker to predict prognosis and tumor immunity in glioma patients, Oncologie (2023), https://doi.org/10.1515/oncologie-2023-0292.

[14] S.J. Dixon, K.M. Lemberg, M.R. Lamprecht, et al., Ferroptosis: an iron-dependent form of nonapoptotic cell death, Cell 149 (5) (May 25 2012) 1060–1072, https://doi.org/10.1016/j.cell.2012.03.042.

[15] Y. Fang, X. Chen, Q. Tan, H. Zhou, J. Xu, Q. Gu, Inhibiting ferroptosis through disrupting the NCOA4-FTH1 interaction: a new mechanism of action, ACS Cent. Sci. 7 (6) (2021) 980–989, https://doi.org/10.1021/acscentsci.0c01592.

[16] W. Tonnus, C. Meyer, C. Steinebach, et al., Dysfunction of the key ferroptosis-surveilling systems hypersensitizes mice to tubular necrosis during acute kidney injury, Nat. Commun. 12 (1) (2021) 4402, https://doi.org/10.1038/s41467-021-24712-6.

[17] K. Bersuker, J.M. Hendricks, Z. Li, et al., The CoQ oxidoreductase FSP1 acts parallel to GPX4 to inhibit ferroptosis, Nature. Nov 575 (7784) (2019) 688–692, https://doi.org/10.1038/s41586-019-1705-2.

[18] M.J. Hangauer, V.S. Viswanathan, M.J. Ryan, et al., Drug-tolerant persister cancer cells are vulnerable to GPX4 inhibition, Nature. Nov 9 551 (7679) (2017) 247–250, https://doi.org/10.1038/nature24297.

[19] I.C. Su, Y.K. Su, S.A. Setiawan, et al., NADPH oxidase subunit CYBB confers chemotherapy and ferroptosis resistance in mesenchymal glioblastoma via nrf2/SOD2 modulation, Int. J. Mol. Sci. (9) (2023) 24, https://doi.org/10.3390/ijms24097706.

[20] C. Bao, J. Zhang, S.Y. Xian, F. Chen, MicroRNA-670-3p suppresses ferroptosis of human glioblastoma cells through targeting ACSL4, Free Radic. Res. 55 (7) (2021) 853–864, https://doi.org/10.1080/10715762.2021.1962009.

[21] J. Cheng, Y.Q. Fan, B.H. Liu, H. Zhou, J.M. Wang, Q.X. Chen, ACSL4 suppresses glioma cells proliferation via activating ferroptosis, Oncology reports. Jan 43 (1) (2020) 147–158, https://doi.org/10.3892/or.2019.7419.

[22] Q. Song, S. Peng, Z. Sun, X. Heng, X. Zhu, Temozolomide drives ferroptosis via a DMT1-dependent pathway in glioblastoma cells, Yonsei Med. J. 62 (9) (Sep 2021) 843–849, https://doi.org/10.3349/ymj.2021.62.9.843.

[23] Y. Zhang, Y. Kong, Y. Ma, et al., Loss of COPZ1 induces NCOA4 mediated autophagy and ferroptosis in glioblastoma cell lines, Oncogene. Feb 40 (8) (2021) 1425–1439, https://doi.org/10.1038/s41388-020-01622-3.

[24] H. Chen, C. Xu, Q. Yu, et al., Comprehensive landscape of STEAP family functions and prognostic prediction value in glioblastoma, J. Cell. Physiol. 236 (4) (Apr 2021) 2988–3000, https://doi.org/10.1002/jcp.30060.

[25] L. Han, L. Bai, X. Fang, et al., SMG9 drives ferroptosis by directly inhibiting GPX4 degradation, Biochem. Biophys. Res. Commun. 567 (Aug 27 2021) 92–98, https://doi.org/10.1016/j.bbrc.2021.06.038.

[26] X. Jin, J. Yin, H. Zhu, et al., SMG9 serves as an oncogene to promote the tumor progression via EMT and wnt/β-catenin signaling pathway in hepatocellular carcinoma, Front. Pharmacol. 12 (2021) 701454, https://doi.org/10.3389/fphar.2021.701454.

[27] Z. Zhao, K.N. Zhang, Q. Wang, et al., Chinese glioma Genome Atlas (CGGA): a comprehensive resource with functional genomic data from Chinese glioma patients, Genomics, proteomics & bioinformatics. Feb 19 (1) (2021) 1–12, https://doi.org/10.1016/j.gpb.2020.10.005.

[28] N. Zhou, X. Yuan, Q. Du, et al., FerrDb V2: update of the manually curated database of ferroptosis regulators and ferroptosis-disease associations, Nucleic Acids Res. (Oct 28 2022), https://doi.org/10.1093/nar/gkac935.

[29] J. Qiu, C. Wang, H. Hu, S. Chen, X. Ding, Y. Cai, Transcriptome analysis and prognostic model construction based on splicing profiling in glioblastoma, Oncology letters. Feb 21 (2) (2021) 138, https://doi.org/10.3892/ol.2020.12399.

[30] Q.T. Ostrom, H. Gittleman, P. Farah, et al., CBTRUS statistical report: primary brain and central nervous system tumors diagnosed in the United States in 2006-2010. Neuro-oncology, Nov 15 (Suppl 2) (2013) ii1–56, https://doi.org/10.1093/neuonc/not151.

[31] B. Zhang, Q. Wu, R. Xu, et al., The promising novel biomarkers and candidate small molecule drugs in lower-grade glioma: evidence from bioinformatics analysis of high-throughput data, J. Cell. Biochem. 120 (9) (2019) 15106–15118, https://doi.org/10.1002/jcb.28773.

[32] Q.T. Ostrom, H. Gittleman, P. Liao, et al., CBTRUS Statistical Report: primary brain and other central nervous system tumors diagnosed in the United States in 2010-2014, Neuro Oncol. 19 (2017) v1–v88, https://doi.org/10.1093/neuonc/nox158 (suppl_5).

[33] W. Renjie, J. Ruichao, D. Junqiang, L. Nan, L. Haiqian, Exosomal circular RNA NT5E driven by heterogeneous nuclear ribonucleoprotein A1 induces temozolomide resistance by targeting microRNA-153 in glioma cells, Oncologie (2023), https://doi.org/10.1515/oncologie-2023-0256.

[34] D.N. Louis, A. Perry, G. Reifenberger, et al., The 2016 World Health organization classification of tumors of the central nervous system: a summary, Acta Neuropathol. 131 (6) (2016) 803–820, https://doi.org/10.1007/s00401-016-1545-1.

[35] D.N. Louis, A. Perry, P. Wesseling, et al., The 2021 WHO classification of tumors of the central nervous system: a summary, Neuro Oncol. 23 (8) (2021) 1231–1251, https://doi.org/10.1093/neuonc/noab106.

[36] L. Gong, M. Jia, ABCC8 is correlated with immune cell infiltration and overall survival in lower grade glioma, Biocell 47 (1) (2023).

[37] A. Yamashita, N. Izumi, I. Kashima, et al., SMG-8 and SMG-9, two novel subunits of the SMG-1 complex, regulate remodeling of the mRNA surveillance complex during nonsense-mediated mRNA decay, Genes & development. 23 (9) (2009) 1091–1105, https://doi.org/10.1101/gad.1767209.

[38] A. Deniaud, M. Karuppasamy, T. Bock, et al., A network of SMG-8, SMG-9 and SMG-1 C-terminal insertion domain regulates UPF1 substrate recruitment and phosphorylation, Nucleic Acids Res. 43 (15) (2015) 7600–7611, https://doi.org/10.1093/nar/gkv668.

[39] S. Nasif, L. Contu, O. Mühlemann, Beyond quality control: the role of nonsense-mediated mRNA decay (NMD) in regulating gene expression. Seminars in cell & developmental biology, Mar 75 (2018) 78–87, https://doi.org/10.1016/j.semcdb.2017.08.053.

[40] R.G.H. Lindeboom, M. Vermeulen, B. Lehner, F. Supek, The impact of nonsense-mediated mRNA decay on genetic disease, gene editing and cancer immunotherapy, Nature genetics. Nov 51 (11) (2019) 1645–1651, https://doi.org/10.1038/s41588-019-0517-5.

[41] T. Kurosaki, M.W. Popp, L.E. Maquat, Quality and quantity control of gene expression by nonsense-mediated mRNA decay, Nature reviews Molecular cell biology. Jul 20 (7) (2019) 406–420, https://doi.org/10.1038/s41580-019-0126-2.

[42] M.W. Popp, L.E. Maquat, Nonsense-mediated mRNA decay and cancer, Current opinion in genetics & development. Feb 48 (2018) 44–50, https://doi.org/10.1016/j.gde.2017.10.007.

[43] G. Nogueira, R. Fernandes, J.F. García-Moreno, L. Romão, Nonsense-mediated RNA decay and its bipolar function in cancer, Mol. Cancer 20 (1) (Apr 29 2021) 72, https://doi.org/10.1186/s12943-021-01364-0.

[44] E. Lion, E.L. Smits, Z.N. Berneman, V.F. Van Tendeloo, NK cells: key to success of DC-based cancer vaccines? Oncol. 17 (10) (2012) 1256–1270, https://doi.org/10.1634/theoncologist.2011-0122.
[45] C. Lee-Chang, M.S. Lesniak, Next-generation antigen-presenting cell immune therapeutics for gliomas, J. Clin. Invest. (3) (2023) 133, https://doi.org/10.1172/jci163449.
[46] T. Marichal, M. Tsai, S.J. Galli, Mast cells: potential positive and negative roles in tumor biology. Cancer immunology research, Nov 1 (5) (2013) 269–279, https://doi.org/10.1158/2326-6066.Cir-13-0119.
[47] S.J. Galli, N. Gaudenzio, M. Tsai, Mast cells in inflammation and disease: recent progress and ongoing concerns, Annu. Rev. Immunol. 38 (2020) 49–77, https://doi.org/10.1146/annurev-immunol-071719-094903.
[48] S. Shi, L. Ye, X. Yu, K. Jin, W. Wu, Focus on mast cells in the tumor microenvironment: current knowledge and future directions, Biochimica et biophysica acta Reviews on cancer. Jan 1878 (1) (2023) 188845, https://doi.org/10.1016/j.bbcan.2022.188845.